



## MATERIALS SCIENCE

# Light-driven directional ion transport for enhanced osmotic energy harvesting

Kai Xiao <sup>1,\*</sup>, Paolo Giusto<sup>1</sup>, Fengxiang Chen<sup>2,5,\*</sup>, Ruotian Chen<sup>3</sup>, Tobias Heil <sup>1</sup>, Shaowen Cao<sup>1,4</sup>, Lu Chen<sup>1,2</sup>, Fengtao Fan<sup>3</sup> and Lei Jiang<sup>2</sup>

## ABSTRACT

Light-driven ion (proton) transport is a crucial process both for photosynthesis of green plants and solar energy harvesting of some archaea. Here, we describe use of a  $\text{TiO}_2/\text{C}_3\text{N}_4$  semiconductor heterojunction nanotube membrane to realize similar light-driven directional ion transport performance to that of biological systems. This heterojunction system can be fabricated by two simple deposition steps. Under unilateral illumination, the  $\text{TiO}_2/\text{C}_3\text{N}_4$  heterojunction nanotube membrane can generate a photocurrent of about  $9 \mu\text{A}/\text{cm}^2$ , corresponding to a pumping stream of  $\sim 5500$  ions per second per nanotube. By changing the position of  $\text{TiO}_2$  and  $\text{C}_3\text{N}_4$ , a reverse equivalent ionic current can also be realized. Directional transport of photogenerated electrons and holes results in a transmembrane potential, which is the basis of the light-driven ion transport phenomenon. As a proof of concept, we also show that this system can be used for enhanced osmotic energy generation. The artificial light-driven ion transport system proposed here offers a further step forward on the roadmap for development of ionic photoelectric conversion and integration into other applications, for example water desalination.

**Keywords:** ion pump, ion transport, nanofluidic, porous membrane, carbon nitride

## INTRODUCTION

Nature's biochemical machinery is a source of inspiration for development of artificial molecular devices or ion transport systems designed to emulate the form and function of their biological counterparts. A typical example is that the cellular metabolism in living organisms depends on the compartmentalization of ions, small molecules and macromolecules being maintained and managed by means of transmembrane active transport. Inspired by this, artificial systems have been developed that are capable of transporting molecules against concentration gradients, such as molecular motors [1,2] and molecular pumps [3]. Photosynthesis by green plants or archebacter is the most important biochemical process in nature, providing most of the energy we need and a comfortable environment suitable for biological survival. With the development of modern science, photosynthesis-inspired light-driven physical and chemical processes have attracted extraordinary attention. We mention, for

instance, photocatalytic chemical reactions [4] or the photovoltaic cell [5], both of which occupy thousands of research groups globally and have already created tremendous economic value. However, artificial photosynthesis involving complex physical and chemical processes is still one of the most tough, but also promising, missions in the field of bionics [6–9].

In terms of energy harvesting, artificial light-driven ion transport is very attractive because the different photosynthetic processes of both green plants and halobacteria involve a step during which protons/ions are pumped from low concentration to high concentration to create an electrochemical potential, which is then used for ATPase to produce ATP. Consequently, the realization of artificial light-driven ion transport is the key point for a new 'ionic' mode of solar energy harvesting and storage [10].

Remarkable progress has also been achieved toward realization of permselectivity of protons or alkaline earth metal ions across membranes by light-induced charge separation [11–13], photoisomerization [14,15] and solid-state nanochannels

<sup>1</sup>Max Planck Institute of Colloids and Interfaces, Department of Colloid Chemistry, Potsdam D-14476, Germany;

<sup>2</sup>Key Laboratory of Bio-inspired Smart Interfacial Science and Technology of Ministry of Education, School of Chemistry, Beihang University, Beijing 100191, China;

<sup>3</sup>State Key Laboratory of Catalysis, 2011-iChEM, Dalian National Laboratory for Clean Energy (DNL), Dalian Institute of Chemical Physics (DICP), Chinese Academy of Sciences, Dalian 116023, China;

<sup>4</sup>State Key Laboratory of Advanced Technology for Materials Synthesis and Processing, Wuhan University of Technology, Wuhan 430070, China and

<sup>5</sup>State Key Laboratory of New Textile Materials and Advanced Processing Technologies, Wuhan Textile University, Wuhan 430200, China

\*Corresponding authors. E-mails: [xiaokai@iccas.ac.cn](mailto:xiaokai@iccas.ac.cn); [fxchen\\_czx@buaa.edu.cn](mailto:fxchen_czx@buaa.edu.cn)

Received 2 June 2020; Revised 10 August 2020;

Accepted 11 August 2020

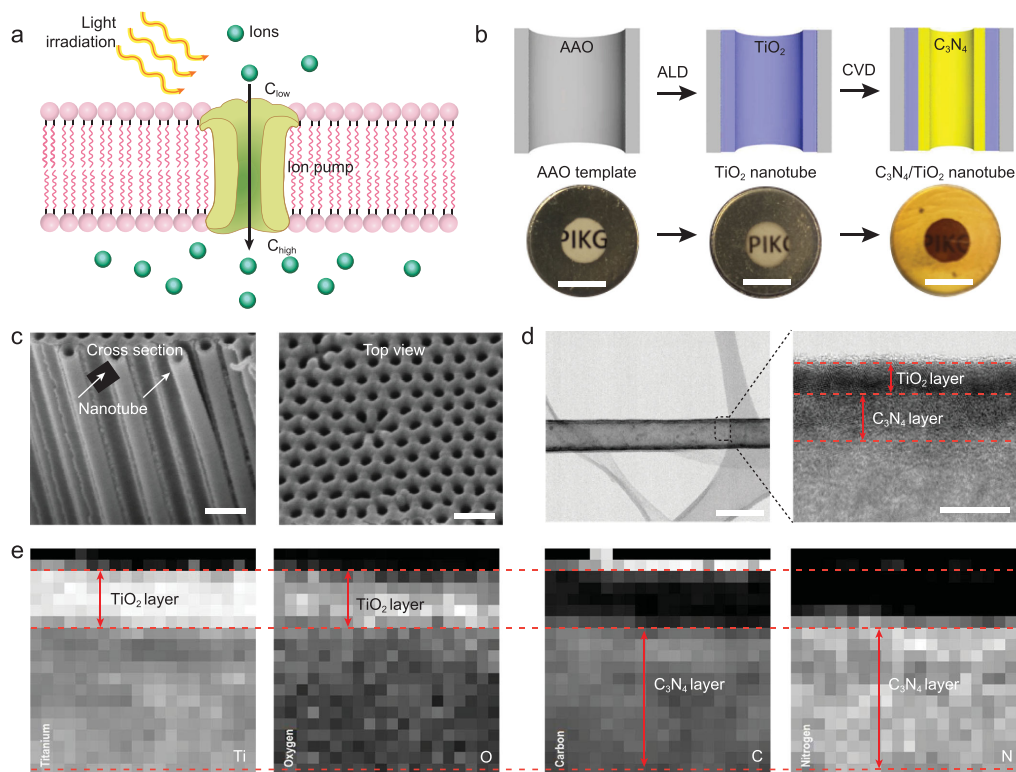


**Figure 1.** Fabrication process and characterization of  $\text{TiO}_2/\text{C}_3\text{N}_4$  semiconductor heterojunction nanotubes. (a) Simplified schematic of light-driven ion transport system. (b) Fabrication process of  $\text{TiO}_2/\text{C}_3\text{N}_4$  heterojunction nanotubes including two steps. Step 1:  $\text{TiO}_2$  layer deposition by ALD; Step 2:  $\text{C}_3\text{N}_4$  layer deposition by CVD (scale bar, 0.5 cm). (c) SEM images of  $\text{TiO}_2/\text{C}_3\text{N}_4$  heterojunction nanotube membrane from cross section and top view (scale bar, 200 nm). (d) TEM image of signal  $\text{TiO}_2/\text{C}_3\text{N}_4$  nanotube (scale bar, 100 nm) and enlarged wall surface (scale bar, 10 nm). (e) Elemental maps of  $\text{TiO}_2/\text{C}_3\text{N}_4$  heterojunction nanotube wall. Each pixel covers  $1 \text{ nm}^2$ .

[16,17]. This ability raises a pertinent question for artificial light-driven ion transport systems: is there a way to drive ion transport by light in an easy and universal manner, and then realize an efficient ‘ionic’ energy harvesting as in nature? Herein, we report development of an artificial light-driven ion transport system via a semiconductor heterojunction nanotube membrane that drives ion transport in a specific direction under unidirectional illumination for photocurrent generation (Fig. 1a). We demonstrate that such semiconductor heterojunction nanotubes consisting of titanium oxide ( $\text{TiO}_2$ ) and polymeric carbon nitride ( $\text{C}_3\text{N}_4$ ) enable efficient light-driven ion transport and tunable ion transport direction by controlling the heterojunction structure.

## RESULTS AND DISCUSSION

### Fabrication and characterization of $\text{TiO}_2/\text{C}_3\text{N}_4$ heterojunction nanotubes

The heterojunction of the semiconductor nanotubes used here is a  $\text{TiO}_2/\text{C}_3\text{N}_4$  heterojunction, which

was fabricated by two deposition steps (Fig. 1b and Supplementary Fig. 1). In the first step,  $\text{TiO}_2$  nanotubes with various wall thicknesses were fabricated by an atom layer deposition (ALD) method using porous anodic aluminum oxide (AAO) membrane with pore diameter about 100 nm as the substrate (Supplementary Fig. 2). Then, the amorphous  $\text{TiO}_2$  nanotubes were crystallized by thermal annealing at  $500^\circ\text{C}$  for 2 hours. In the second step, the anatase  $\text{TiO}_2$  nanotubes (Supplementary Fig. 3) were coated with a 10 nm layer of  $\text{C}_3\text{N}_4$  (Supplementary Fig. 4) by chemical vapor deposition (CVD) [18]. In this way, a  $\text{TiO}_2/\text{C}_3\text{N}_4$  heterojunction nanotube was fabricated (Fig. 1c). For analytical reasons, the carbon nitride nanotube can be released by chemical etching of the AAO substrate by 5 wt% phosphoric acid. Figure 1d shows a typical TEM image of a  $\text{TiO}_2/\text{C}_3\text{N}_4$  heterojunction nanotube, with the enlarged wall section showing that the wall is composed of an inner  $\text{TiO}_2$  layer and outer  $\text{C}_3\text{N}_4$  layer. High-resolution EDX measurements of the partial wall section in Fig. 1e and Supplementary Fig. 5 show that the inner  $\text{TiO}_2$  layer is about 5 nm thick, while the outer  $\text{C}_3\text{N}_4$  layer is about

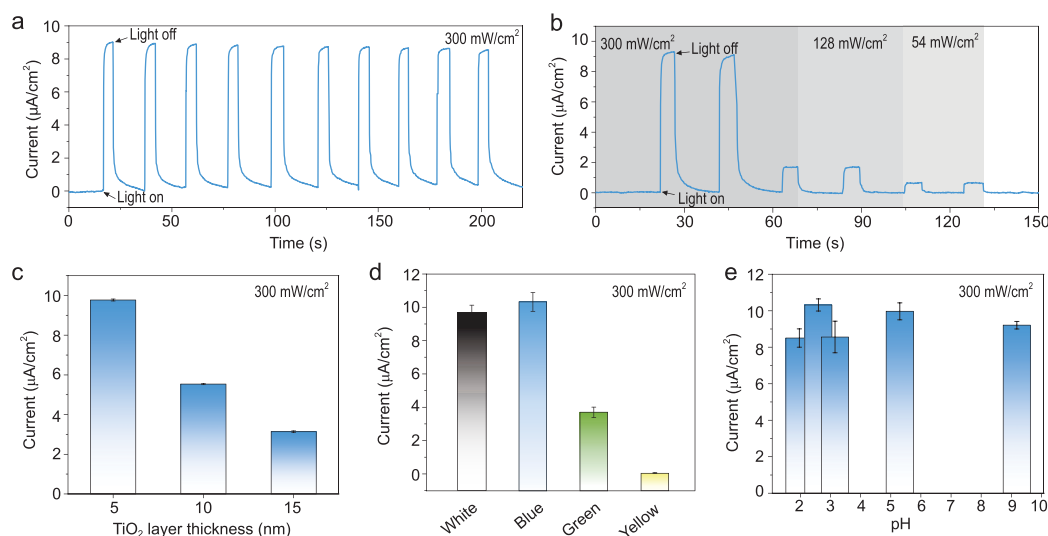


**Figure 2.** Light-driven ion transport performance of  $\text{TiO}_2/\text{C}_3\text{N}_4$  semiconductor heterojunction nanotube membrane. (a) Measured cyclic constant zero-volt current with alternating illumination at 0.1 M KCl concentration. (b) Zero-volt current as a function of light density of  $54 \text{ mW}/\text{cm}^2$ ,  $128 \text{ mW}/\text{cm}^2$  and  $300 \text{ mW}/\text{cm}^2$ . (c) Zero-volt current as a function of  $\text{TiO}_2$  layer thickness. (d) Zero-volt current as a function of monochromatic light (blue:  $405 \text{ nm}$ ; green:  $515 \text{ nm}$ ; yellow:  $590 \text{ nm}$ ) with same power density of  $300 \text{ mW}/\text{cm}^2$ . The ionic current is consistent with the light absorbance of outer  $\text{C}_3\text{N}_4$  layer. (e) Zero-volt current as a function of pH. Error bars in (c–e) represent the standard deviations of five independent experiments.

10 nm thick (The pixel intensity represents the concentration of the related elements, respectively. Each pixel covers  $1 \text{ nm}^2$ ). This is a representative of samples used in this work, but the thickness of the  $\text{C}_3\text{N}_4$  and  $\text{TiO}_2$  layers can be well controlled (see below). The length of all samples is the same, about  $60 \mu\text{m}$ . The obtained heterojunction nanotubes were investigated by X-ray diffraction (XRD) measurements, FT-IR spectroscopy and X-ray photoelectron spectroscopy (XPS) (Supplementary Figs 6–8). All of the results indicate formation of  $\text{TiO}_2/\text{C}_3\text{N}_4$  heterojunction nanotubes.

### Light-driven ion transport phenomenon

The light-driven ion transport properties were measured using a home-made electrolyte cell, as we have reported previously [19,20]. The  $\text{TiO}_2/\text{C}_3\text{N}_4$  heterojunction nanotube membrane was symmetrically placed in contact with a 0.1 M KCl solutions and initially illuminated from one side. Figure 2a shows the cycle-constant zero-volt current across the nanotube membrane by simulated solar illumination of  $300 \text{ mW}/\text{cm}^2$ . Without illumination, the zero-volt current is almost zero, while it increased to about  $9 \mu\text{A}/\text{cm}^2$  with illumination, indicating that light provides an external force to drive ions to move. By calculation, the changed current translates into the fact that a single nanotube actively transports  $\sim 5500$  ions per second, an unprecedented breakthrough for artificial light-driven

ion transport systems and much closer to values for the bacteriorhodopsin sodium pump [21] or halorhodopsin Cl ion pump [22]. The directional photo-driven ion transport phenomenon can be directly confirmed by the change of ion concentration in the two cells (Supplementary Fig. 9), which can be monitored in real time with a scanning ion-selective electrode technique (SIET). In addition, the membrane shows an instantaneous stable and fully repeatable response to illumination. The ionic current is still stable even at longer illumination (Supplementary Fig. 10). Further measurements show that the ion transport is closely connected to the illumination power density. The dependence can be confirmed by the ionic current shown in Fig. 2b. With decrease of power density from  $300 \text{ mW}/\text{cm}^2$  to  $54 \text{ mW}/\text{cm}^2$ , the ionic current decreases gradually from  $9 \mu\text{A}/\text{cm}^2$  to  $0.8 \mu\text{A}/\text{cm}^2$ . It is worth mentioning that the photo-induced voltage is also positively correlated with light power density (Supplementary Fig. 9), while it is only dozens of millivolts and much smaller than that for pure  $\text{C}_3\text{N}_4$  nanotube membrane [20].

The wall thickness of  $\text{TiO}_2$  nanotube has an obvious effect on the light-driven ion transport properties (Fig. 2c). With increase of wall thickness from 5 nm to 15 nm (Supplementary Fig. 2), the ionic current decreases from about  $9 \mu\text{A}/\text{cm}^2$  to  $2.5 \mu\text{A}/\text{cm}^2$ . This could be ascribed to a less efficient photochemical charge separation and more interfacial recombination of electrons and holes in

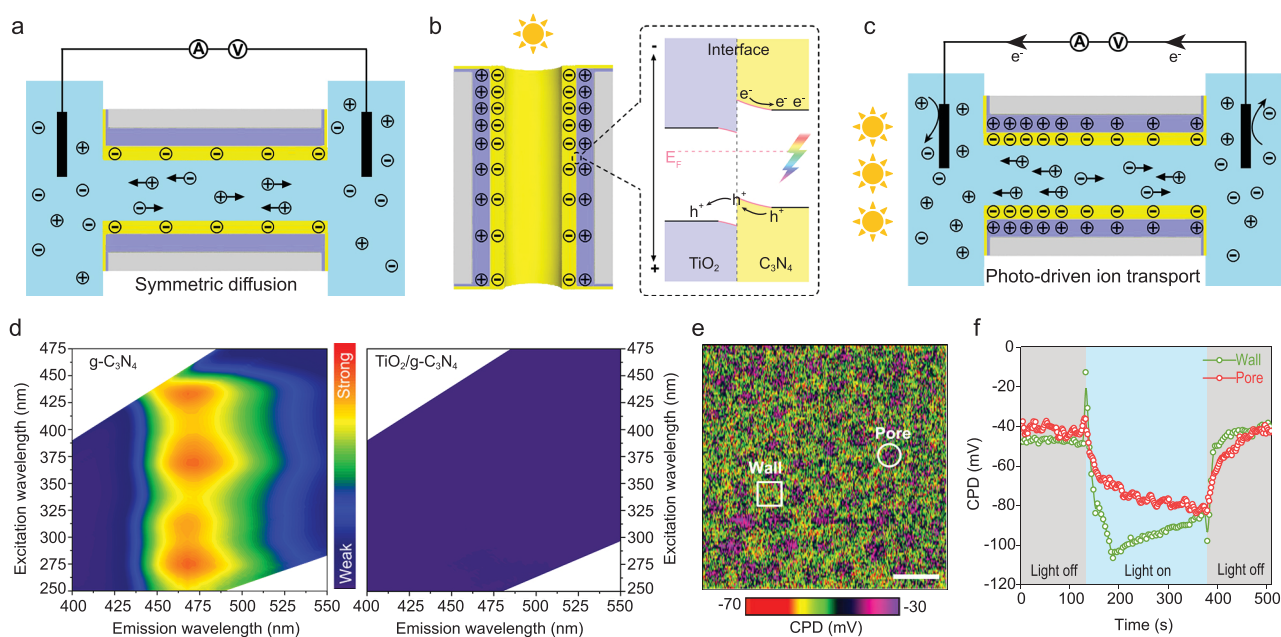


**Figure 3.** Mechanism of light-driven ion transport phenomenon. (a) Schematic of the surface charge distribution on the nanotube before illumination, in which condition low density negative charge is homogeneously distributed over the nanotube. (b) Light-induced separation of electrons and holes of C<sub>3</sub>N<sub>4</sub>. The holes transfer from C<sub>3</sub>N<sub>4</sub> to TiO<sub>2</sub>. (c) Schematic of the surface charge distribution on the nanotube after unilateral illumination, in which condition the separation of electrons and holes results in heterogeneous negative charge distribution. (d) Fluorescent mapping of C<sub>3</sub>N<sub>4</sub> (left) and TiO<sub>2</sub>/C<sub>3</sub>N<sub>4</sub> (right) nanotube membranes. (e) KPFM image of the TiO<sub>2</sub>/C<sub>3</sub>N<sub>4</sub> nanotube membranes. Scale bar, 200 nm. (f) Surface potential (CPD) evolution with light on and off in pore area and wall area of the TiO<sub>2</sub>/C<sub>3</sub>N<sub>4</sub> nanotube.

thicker case [23]. The light-driven ion transport system also shows an obvious relationship with the light wavelength (Fig. 2d). When applying various monochromatic light with the same power density (300 mW/cm<sup>2</sup>), white light and high-energy blue light have a comparable high ‘power’ to drive ion transport, while low-energy green and yellow light show a much weaker effect (Supplementary Fig. 11). This is consistent with the light absorbance of the exposed C<sub>3</sub>N<sub>4</sub> layer (Supplementary Fig. 12) [24]. In general, the isoelectric point of C<sub>3</sub>N<sub>4</sub> fabricated by different precursors is in the range of 3.5 to 5 [25], while the light-driven ion transport system is universal and works constantly in a wider pH value range from 1.9 to 9.5 (Fig. 2e). In strong alkali solution with a pH value of 12.5 it shows a different phenomenon as C<sub>3</sub>N<sub>4</sub> is surface-hydrolyzed under such conditions (Supplementary Fig. 13) [26,27]. Meanwhile, the ionic current shows a positive correlation with electrolyte concentration (Supplementary Fig. 14).

### Mechanism of light-driven ion transport

The surface charge redistribution of the heterojunction nanotube resulting from photo-induced separation of electrons and holes is thought to be key

to the light-driven ion transport phenomenon. As illustrated in Fig. 3a, the initial TiO<sub>2</sub>/C<sub>3</sub>N<sub>4</sub> nanotube has a symmetric weakly negative charge because of the acidity of the inner C<sub>3</sub>N<sub>4</sub> layer [28]. In this condition, there is no ionic current in the external circuit. When illuminated from one side of the H-cell, the surface charge density on the irradiated side of the TiO<sub>2</sub>/C<sub>3</sub>N<sub>4</sub> nanotube increases because the built-in potential in the heterojunction resulting from band bending will drive photogenerated holes to move from the C<sub>3</sub>N<sub>4</sub> layer to the TiO<sub>2</sub> layer (Fig. 3b). This results in a positively charged TiO<sub>2</sub> layer and a negatively charged C<sub>3</sub>N<sub>4</sub> layer. As the asymmetric negative surface charge is created, cations will move from the non-illuminated side to the illuminated side, while anions move oppositely (Fig. 3c). In this way, a light-driven ion transport system develops. Previous work has already shown that a single phase C<sub>3</sub>N<sub>4</sub> nanotube exhibits similar, but weaker, light-driven ion transport properties [20,29], caused by less efficient photocharge separation [30,31]. In the present system, the nanoscopic TiO<sub>2</sub>/C<sub>3</sub>N<sub>4</sub> heterojunction structure provides two different phases for each charge. The proposed mechanism is further confirmed by fluorescent mapping. As shown in Fig. 3d, the fluorescent mapping of the C<sub>3</sub>N<sub>4</sub> nanotube system (left) exhibited fluorescence signals, which



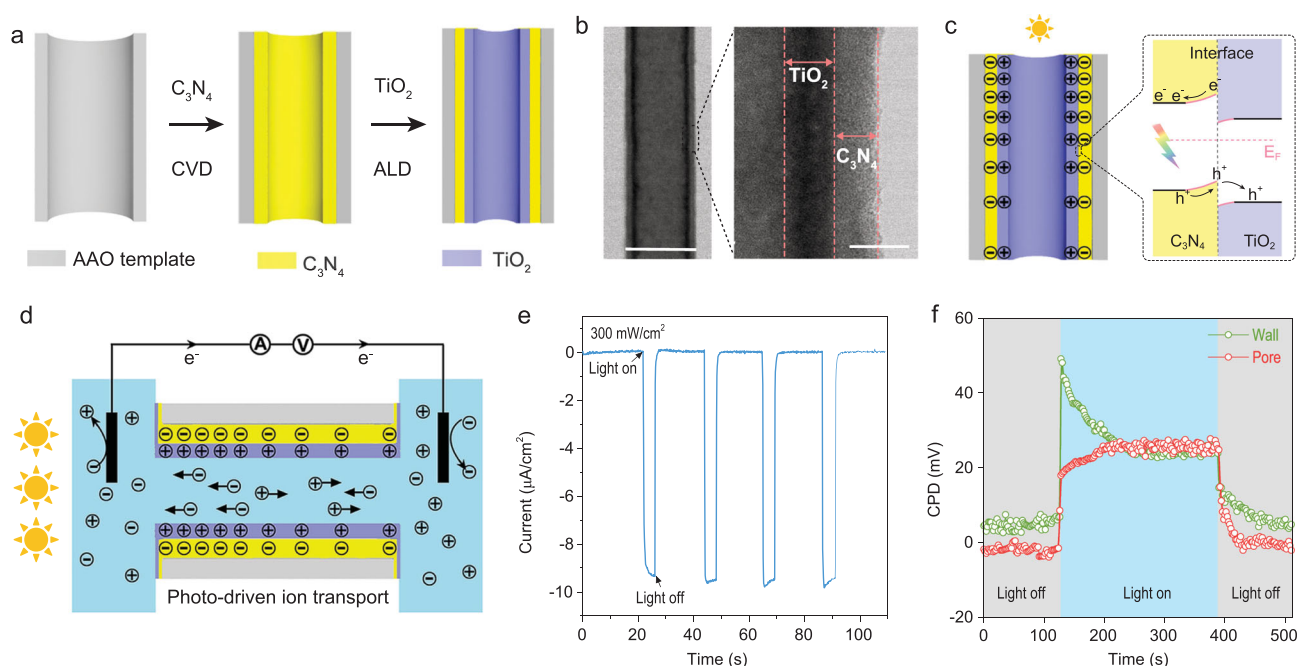


**Figure 4.** Fabrication of  $C_3N_4/TiO_2$  heterojunction nanotubes and their performance. (a) Schematic fabrication process of the  $C_3N_4/TiO_2$  heterojunction nanotube. Step 1:  $C_3N_4$  layer deposition by CVD; Step 2:  $TiO_2$  layer deposition by ALD. (b) TEM image of signal  $C_3N_4/TiO_2$  nanotube (scale bar, 100 nm) and enlarged wall surface (scale bar, 10 nm). (c) Light-induced separation of electrons and holes of  $C_3N_4$ . The holes will transfer from  $C_3N_4$  to  $TiO_2$ . (d) Schematic of surface charge distribution and ion transport in the nanotube after unilateral illumination. (e) Measured cyclic constant zero-volt current with alternating illumination. (f) CPD evolution with light on and off in pore area and wall area of  $C_3N_4/TiO_2$  nanotube.

represent recombination of photo-generated electrons and holes; whereas for the  $TiO_2/C_3N_4$  heterojunction system (right), the fluorescence is negligible (Supplementary Fig. 15), which means that radiative recombination is effectively suppressed in the heterojunction structure.

To directly observe the charge distribution, we mapped the surface potential by Kelvin probe force microscopy (KPFM) under unilateral illumination. For the  $C_3N_4$  nanotube, the potential of the pore area is 40 mV lower than that of the wall area, indicating upward band bending and electron capture by the  $C_3N_4$  nanotube surface. Meanwhile, light irradiation increased the surface potential in both areas, indicating the n-type semiconductor property of  $C_3N_4$  (Supplementary Fig. 16). As for the  $TiO_2/C_3N_4$  heterojunction structure, the surface potential of the pore area exceeds that of the wall area by 10 mV (Fig. 3e and Supplementary Fig. 17), indicating band bending and generation of built-in electrical field in the heterojunction. After light irradiation, the surface potentials of both the pore area and the wall area decreased, giving direct evidence for directional transport of photogenerated electrons (to the outer  $C_3N_4$  layer) and holes (to the inner  $TiO_2$  layer) (Fig. 3f). The observed electron accumulation at the illuminated side both on the wall and in the pore coincides with the measured cation

migration towards the illuminated surface (Fig. 3c), thus indicating that the light-induced charge redistribution is responsible for the driving force of ion migration [32].

### Reverse ion transport by $C_3N_4/TiO_2$ heterojunction nanotubes

The light-driven ion transport can also be easily reversed by changing the position of  $C_3N_4$  and  $TiO_2$ . We fabricated a second  $C_3N_4/TiO_2$  nanotube membrane by the same deposition methods but with reverse order (Fig. 4a). Now,  $C_3N_4$  is placed in the inner layer and  $TiO_2$  in the outer layer. Figure 4b shows a typical TEM image of the  $C_3N_4/TiO_2$  heterojunction nanotube and the enlarged wall section shows clearly that the wall is composed by an inner  $C_3N_4$  layer and an outer  $TiO_2$  layer, both of which have a thickness of about 7 nm (a representative sample). With the unilateral illumination, the outer  $TiO_2$  layer should be positively charged from the directional movement of photogenerated holes (Fig. 4c). In this way, the anions will move from the non-illuminated side to the illuminated side (Fig. 4d). Figure 4e shows the cyclic constant zero-volt current across the nanotube membrane under a simulated solar illumination of  $300 \text{ mW/cm}^2$ . Without illumination, the zero-volt current is almost

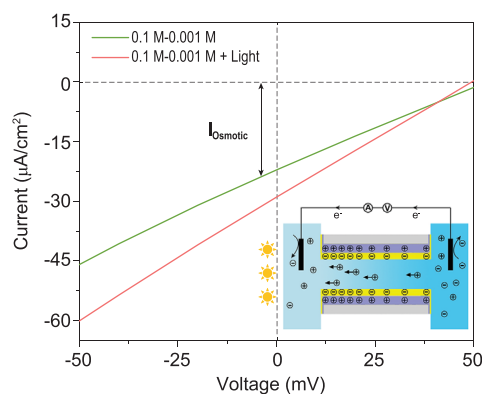


**Figure 5.** Potential application of photo-driven ion transport for enhanced osmotic energy generation. The typical current–voltage curves before and after light ( $300 \text{ mW/cm}^2$ ) irradiation at 100-fold ( $C_H = 0.1 \text{ M}$ ;  $C_L = 0.001 \text{ M}$ ) KCl concentration gradient.

zero, while it increased to about  $-9 \mu\text{A/cm}^2$  under illumination, which indicates that light provides an opposite external force for ion pumping. Figure 4f shows clearly that the reverse  $\text{C}_3\text{N}_4/\text{TiO}_2$  combination yields an opposite transmembrane photovoltage compared to the  $\text{TiO}_2/\text{C}_3\text{N}_4$  combination (Fig. 3f), in agreement with the reversed ion transport performance and further confirming the mechanism of light-driven ion transport. We can assume that not only can the ion transport direction be directly controlled using different semiconductor heterojunction combinations, but also the photocurrent value can be adjusted by combining different semiconductors with suitable band gaps. This suggests that semiconductor heterojunction nanotubes are a universal way to realize light-driven ion transport.

### Photo-enhanced blue energy generation

Beyond providing a novel method for photoelectrical energy conversion, this ion transport system can be potentially integrated into other energy harvesting approaches, for example to harvest salinity gradient energy, also called ‘blue energy’ [33–35]. Blue energy is a sustainable, abundant and inexpensive source of clean energy that is mainly stored in the sheer amount of available fresh and salty water being mixed (e.g. at the Yangtze river muzzle) [36]. The recently developed nanofluidic reverse-electrodialysis (NRED) method provides a very appealing way to harvest this energy and works again by a charged nanochannel or porous nanochannel membranes [10,37]. In the NRED process, surface charge density plays a crucial role. Generally speaking, high surface charge density will boost the blue energy power density. The weakly charged

$\text{TiO}_2/\text{C}_3\text{N}_4$  heterojunction nanotube membrane already can be used to harvest blue energy, but creates an osmotic current of only  $21 \mu\text{A/cm}^2$  employing a 100-fold (0.1 M-0.001 M) concentration gradient (Fig. 5). With  $300 \text{ mW/cm}^2$  light irradiation from the low concentration side, the osmotic current increased to about  $28 \mu\text{A/cm}^2$ . This enhanced osmotic current is ascribed to the increased surface charge density induced by light irradiation, but also to the pumping flux being of the order of the current increase. The present light-driven ion transport system thereby provides an opportunity to integrate solar energy and salinity gradient energy [32], potentially overcoming the disadvantages of low energy efficiency and poor power density currently associated with blue energy.

### CONCLUSION

In summary, we report that semiconductor heterojunction nanotubes, herein using  $\text{TiO}_2/\text{C}_3\text{N}_4$  heterojunction nanotubes as an example, can be used for constructing an artificial light-driven ion transport system, which can then be used for ionic energy generation. The light-driven ionic current can reach up to about  $9 \mu\text{A/cm}^2$ , three times that of  $\text{C}_3\text{N}_4$  nanotubes. The ionic transport direction can easily be reversed by modifying the semiconductor deposition sequence. The enhanced and flexible light-driven ionic current can be ascribed to redistribution of surface charge across nanotubes. In addition, we may expect that other semiconductor or semiconductor heterojunction nanostructures, which are currently used for photocurrent generation, for example two-dimensional van der Waals semiconductors [38] or 2D MOF [39], will exhibit similar light-driven ion transport performance. Most importantly, not only ions but also specific charged organic molecules up to small peptides are expected to be transported with the aid of this novel approach for directed molecular movement.

### SUPPLEMENTARY DATA

Supplementary data are available at [NSR](https://doi.org/10.1093/nsr/nwaa231) online.

### FUNDING

This work was financially supported by the Max Planck Society and National Key Research.

### AUTHOR CONTRIBUTIONS

K.X. conceived, designed and performed the experiments. P.G. performed the CVD and fluorescent mapping. F.X.C performed

the ALD and XPS. T.H. acquired the TEM measurements. R.T.C. helped measure the KPFM and discussed the mechanism. K.X. wrote the manuscript. All authors analyzed the data and discussed the results.

**Conflict of interest statement.** None declared.

## REFERENCES

- Ruangsupapichat N, Pollard MM and Harutyunyan SR *et al.* Reversing the direction in a light-driven rotary molecular motor. *Nat Chem* 2011; **3**: 53–60.
- Li Q, Fuks G and Eoulin M *et al.* Macroscopic contraction of a gel induced by the integrated motion of light-driven molecular motors. *Nat Nanotechnol* 2015; **10**: 161–5.
- Cheng C, McGonigal PR and Schneebeli ST *et al.* An artificial molecular pump. *Nat Nanotechnol* 2015; **10**: 547–53.
- Chen G, Waterhouse GIN and Shi R *et al.* From solar energy to fuels: recent advances in light-driven C1 chemistry. *Angew Chem Int Ed* 2019; **58**: 17528–51.
- Gratzel M. Photoelectrochemical cells. *Nature* 2001; **414**: 338–44.
- Kornienko N, Zhang J and Sakimoto KK *et al.* Interfacing nature's catalytic machinery with synthetic materials for semi-artificial photosynthesis. *Nat Nanotechnol* 2018; **13**: 890–9.
- Zhang H, Liu H and Tian Z *et al.* Bacteria photosensitized by intracellular gold nanoclusters for solar fuel production. *Nat Nanotechnol* 2018; **13**: 900–5.
- Ong WJ, Tan LL and Ng YH *et al.* Graphitic carbon nitride (g-C<sub>3</sub>N<sub>4</sub>)-based photocatalysts for artificial photosynthesis and environmental remediation: are we a step closer to achieving sustainability? *Chem Rev* 2016; **116**: 7159–329.
- Steinberg-Yfrach G, Liddell P and Hung S-C *et al.* Conversion of light energy to proton potential in liposomes by artificial photosynthetic reaction centres. *Nature* 1997; **385**: 239–41.
- Xiao K, Jiang L and Antonietti M. Ion transport in nanofluidic devices for energy harvesting. *Joule* 2019; **3**: 2364–80.
- Bhosale S, Sisson A and Talukdar P *et al.* Photoproduction of proton gradients with pi-stacked fluorophore scaffolds in lipid bilayers. *Science* 2006; **313**: 84–6.
- Steinberg-Yfrach G, Rigaud J-L and Durantini E *et al.* Light-driven production of ATP catalysed by F<sub>0</sub>F<sub>1</sub>-ATP synthase in an artificial photosynthetic membrane. *Nature* 1998; **392**: 479–82.
- Gust D, Moore TA and Moore AL. Mimicking photosynthetic solar energy transduction. *Acc Chem Res* 2001; **34**: 40–8.
- Xie X, Crespo GA and Mistlberger G *et al.* Photocurrent generation based on a light-driven proton pump in an artificial liquid membrane. *Nat Chem* 2014; **6**: 202–7.
- Xie X and Bakker E. Photoelectric conversion based on proton-coupled electron transfer reactions. *J Am Chem Soc* 2014; **136**: 7857–60.
- Zhang Z, Li P and Kong X-Y *et al.* Bioinspired heterogeneous ion pump membranes: unidirectional selective pumping and controllable gating properties stemming from asymmetric ionic group distribution. *J Am Chem Soc* 2018; **140**: 1083–90.
- Zhang Z, Kong X-Y and Xie G *et al.* "Uphill" cation transport: a bioinspired photo-driven ion pump. *Sci Adv* 2016; **2**: e1600689.
- Giusto P, Cruz D and Heil T *et al.* Shine bright like a diamond: new light on an old polymeric semiconductor. *Adv Mater* 2020; **32**: 1908140.
- Xiao K, Giusto P and Wen L *et al.* Nanofluidic ion transport and energy conversion through ultrathin free-standing polymeric carbon nitride membranes. *Angew Chem Int Ed* 2018; **57**: 10123–6.
- Xiao K, Chen L and Chen R *et al.* Artificial light-driven ion pump for photoelectric energy conversion. *Nat Commun* 2019; **10**: 74.
- Inoue K, Ono H and Abe-Yoshizumi R *et al.* A light-driven sodium ion pump in marine bacteria. *Nat Commun* 2013; **4**: 1678.
- Bamberg E, Tittor J and Oesterheld D. Light-driven proton or chloride pumping by halorhodopsin. *Proc Natl Acad Sci USA* 1993; **90**: 639–43.
- Subila KB, Sandeep K and Thomas EM *et al.* CdSe-CdTe heterojunction nanorods: role of CdTe segment in modulating the charge transfer processes. *ACS Omega* 2017; **2**: 5150–8.
- Wang X, Maeda K and Thomas A *et al.* A metal-free polymeric photocatalyst for hydrogen production from water under visible light. *Nat Mater* 2009; **8**: 76–80.
- Zhu B, Xia P and Ho W *et al.* Isoelectric point and adsorption activity of porous g-C<sub>3</sub>N<sub>4</sub>. *Appl Surf Sci* 2015; **344**: 188–95.
- Sano T, Tsutsui S and Koike K *et al.* Activation of graphitic carbon nitride (g-C<sub>3</sub>N<sub>4</sub>) by alkaline hydrothermal treatment for photocatalytic NO oxidation in gas phase. *J Mater Chem A* 2013; **1**: 6489–96.
- Tian J, Liu Q and Asiri AM *et al.* Ultrathin graphitic C<sub>3</sub>N<sub>4</sub> nanofibers: hydrolysis-driven top-down rapid synthesis and application as a novel fluorosensor for rapid, sensitive, and selective detection of Fe<sup>3+</sup>. *Sens Actuators B Chem* 2015; **216**: 453–60.
- Li X-H, Zhang J and Chen X *et al.* Condensed graphitic carbon nitride nanorods by nanoconfinement: promotion of crystallinity on photocatalytic conversion. *Chem Mater* 2011; **23**: 4344–8.
- Xiao K, Tu B and Chen L *et al.* Photo-driven ion transport for a photodetector based on an asymmetric carbon nitride nanotube membrane. *Angew Chem Int Ed* 2019; **58**: 12574–9.
- Godin R, Wang Y and Zwijnenburg MA *et al.* Time-resolved spectroscopic investigation of charge trapping in carbon nitrides photocatalysts for hydrogen generation. *J Am Chem Soc* 2017; **139**: 5216–24.
- Merschjann C, Tschierlei S and Tyborski T *et al.* Complementing graphenes: 1D interplanar charge transport in polymeric graphitic carbon nitrides. *Adv Mater* 2015; **27**: 7993–9.
- Graf M, Lihter M and Unuchek D *et al.* Light-enhanced blue energy generation using MoS<sub>2</sub> nanopores. *Joule* 2019; **3**: 1549–64.
- Chen C, Liu D and He L *et al.* Bio-inspired nanocomposite membranes for osmotic energy harvesting. *Joule* 2020; **4**: 247–61.
- Siria A, Poncharal P and Bianco A-L *et al.* Giant osmotic energy conversion measured in a single transmembrane boron nitride nanotube. *Nature* 2013; **494**: 455–8.

35. Siria A, Bocquet M-L and Bocquet L. New avenues for the large-scale harvesting of blue energy. *Nat Rev Chem* 2017; **1**: 0091.
36. Marbach S and Bocquet L. Osmosis, from molecular insights to large-scale applications. *Chem Soc Rev* 2019; **48**: 3102–44.
37. Macha M, Marion S and Nandigana VVR *et al.* 2D materials as an emerging platform for nanopore-based power generation. *Nat Rev Mater* 2019; **4**: 588–605.
38. Buscema M, Island JO and Groenendijk DJ *et al.* Photocurrent generation with two-dimensional van der Waals semiconductors. *Chem Soc Rev* 2015; **44**: 3691–718.
39. Song X, Wang X and Li Y *et al.* 2D semiconducting metal-organic framework thin films for organic spin valves. *Angew Chem Int Ed* 2020; **59**: 1118–23.